Sidescan Sonar Image Processing Techniques

Pierre Cervenka and Christian de Moustier, *Member, IEEE*

Abstract— **A four-step processing sequence is described to produce image mosaics from the various segments of a sidescanned acoustic imaging survey of a given seafloor area. Starting with data consisting for each ping of acoustic backscatter levels versus horizontal range across-track, median prefiltering is used first to reduce the influence of outliers on subsequent linear processes. Artifacts that are clearly unrelated to the backscattering properties of the seafloor are then isolated on a ping by ping basis through a spectral analysis that relies on a decomposition using Chebyshev polynomials to filter the low spatial frequency components of the image. Contrast enhancement is then achieved through an original implementation of the classical gray level histogram equalization technique by balancing local versus global histogram contributions. Finally, pixels are mapped on a geographic grid taking due account of the geometry of the measurement and of the spacing between pings to minimize along-track smearing of features. Examples of results obtained with these processing techniques are given for SeaMARC II data recorded during a complete survey of Fieberling Guyot (32°.5N, 128°W).**

Index Terms—**SeaMARC II, sidescan sonar, image processing.**

I. Introduction

SIDESCAN sonar images of the seafloor typically consist of a series of lines, one per transmission-reception cycle, displayed perpendicularly to the survey track. On each side of the track, a single line segment represents the echoes received from the seafloor for a given ping as a function of slant range (time), or horizontal range if the appropriate corrections for refraction and topography have been used. In addition, a time-varying gain compensates for transmission losses caused by spherical spreading and absorption of sound waves in water. However, if no other corrections are made, the resulting images usually suffer from numerous distortions and artifacts, because: 1) various forms of noise or external interferences, e.g., caused by other acoustic devices operated at the same time, are added to the process; 2) the survey track is rarely straight and the attitude of the tow fish (roll, pitch, yaw) changes with time; 3) the beam patterns of the sonar are not uniform in the angular sector of interest; in addition, their side or back lobes may contribute to cross-talk between the two sides or may pick up echoes reflected from the sea surface. Even free of these impediments, the images may still be difficult to interpret visually because they lack contrast.

A number of image processing techniques, such as noise filtering, radiometric corrections, contrast enhancement, deblurring through constrained iterative deconvolution, and navigation corrections in computer mosaics of multiple swaths, have been implemented to correct or alleviate flaws in the recorded data (e.g., [1]–[10]). In this paper, we expand on these techniques and present a new spatial filter designed to improve the readability of sidescan sonar images of the seafloor, making them more suitable for analysis and interpretation by the end-user than the raw recorded image. We focus on seafloor backscatter image processing issues and describe the main processing steps used in producing the final images. Geometric corrections such as pixel relocation based on bathymetry are addressed in a companion paper [11]. Although the techniques presented here have been developed with data gathered by the SeaMARC II bathymetric sidescan sonar system [12], they are applicable to most other sidescan sonar systems. The dynamic range of the recorded data is assumed to span 256 levels, i.e., 8 bits per datum.

In cleaning images, we are primarily concerned with artifacts appearing as abrupt amplitude changes within a single ping or between adjacent pings. Such artifacts might be the expression of missing data, over all or part of a ping as a result of external interferences, or of bottom detection errors. Some of these artifacts may contribute to the presence of outliers in the upper and lower bins of the gray-level histogram of the image. Other sources of outliers in the histogram include speckle noise and random noise spikes potentially associated with telemetry errors. These outliers must be reduced as much as possible prior to performing any linear filtering, as they are likely to bias the filtering results. We have used conventional median filters [13], [14] for this purpose, and the rationale for this choice is presented in Section I.

Some of the gray-level changes observable in the image are less pronounced, but they give the impression that certain pings have a constant amplitude offset with respect to their neighbors. Such artifacts are most likely caused by the dynamic changes in sonar attitude, primarily yaw and to a lesser extent pitch, that cause the nonuniform beam pattern to sweep in, out, and around during the ping cycle. As the bearing of the sonar changes between transmission and reception, the high azimuthal directivity of the arrays (typically ≤ 2 degree) induces drastic variations in the level of the received signals (Fig. 1). These attitude fluctuations occur while the stream of echoes from the seafloor is being recorded, so that the perturbation is more complicated than a simple offset as mentioned above. However, the yaw and pitch periods are not very small compared with the ping cycle so that the size of the

Manuscript received December 5, 1992; revised March 18, 1993. This work was supported by the Office of Naval Research under Grants N00014-91-J-1073 and N00014-90-J-4009 (subcontract to Hawaii Institute of Geophysics). Part of this paper was presented at the Oceans '91 Conference.

P. Cervenka was with the Marine Physical Laboratory, Scripps Institution of Oceanography, University of California, San Diego, La Jolla, CA 92093-0205; he is currently with the Laboratoire de Mecanique Physique, Universite Pierre et Marie Curie, 78210 Sant-Cyr-l'Ecole, France.

C. deMoustier is with the Marine Physical Laboratory, Scripps Institution of Oceanography, University of California, San Diego, La Jolla, CA 92093-0205.

IEEE Log Number 9209068.

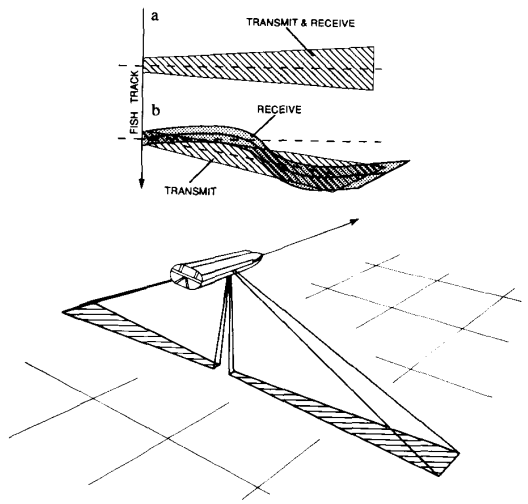

Fig. 1. Effect of fish attitude on the acoustic backscatter geometry. A one-sided insonification pattern is shown for: (a) the ideal case in which transmit and receive beam patterns overlap perfectly and are perpendicular to the track; (b) the transmit beam is not perpendicular to the track and the receive pattern shows the effect of yaw and pitch motions.

resulting multiplicative patterns is not very small compared with the swath width.

We also address artifacts that are nearly invariant in the along-track direction. Incorrect time varying gain corrections, as well as poor or nonexistent beam pattern corrections, lead to across-track variations of signal magnitude that remain coherent along-track over entire traverses. In some instances, the angular dependence of seafloor backscatter produces a similar effect. As in the case of yaw, the resulting across-track patterns are likely to be slowly varying on distances commensurate with the swath width. The correction method presented below is based on this assumption.

A direct approach to removing these artifacts is the causal method whereby deterministic corrections are derived from available parameters such as the recorded position of the sonar in the water column, the estimated propagation losses or the calibrated directivity of the transducers. However, in most cases these causal phenomena are inaccurately quantized and residual artifacts are still visible in the corrected image.

Our approach is purely stochastic and does not require *a priori* knowledge of the fish's attitude or position in the water column. It deals with the low spatial frequency components of the image whose wavelengths are not small compared with the half width of the swath. This method can be implemented directly or at a post-processing stage, i.e., after deterministic corrections have been applied. In Section II, we show how a Chebyshev polynomial decomposition applies to this problem by spectral analysis of the spatial characteristics of the image. The processing algorithm is described in detail.

Although somewhat improved by the previous treatment, backscatter images still need to be enhanced to take advantage of the available gray-level dynamic range. A classical technique consists of stretching the representation by equalization of the gray-level histogram. We present in Section III an implementation that allows balancing of the global rendering of a mosaicked survey with the emphasis upon the local structures.

From a practical point of view, we consider that the port and starboard sides are independent and the corresponding images are treated as if coming from two one-sided systems. This approximation is valid if one excludes the cross-talk effects that are not addressed here. For each side, the image is cropped to a rectangular frame that is filled without data gaps along or across track, so that continuous records can be processed in both perpendicular directions. Images are displayed in terms of horizontal range derived with the classical flat bottom assumption, although the across-track expansion could have been done just as well in terms of slant range; the pertinent fact is that data are framed and fully fit in a rectangle. This rectangular format is required for the median prefiltering and the stochastic linear filtering stages mentioned above. It is also convenient to use for contrast enhancement operations.

At the final stage of the process, pixels are transferred from this generic rectangular format to a geographic grid by taking into account the navigation data. To this end, we describe in Section V a remapping process intended to limit the along-track blurring that commonly results from this operation.

At each step of the processing sequence, the techniques are illustrated with application examples using data recorded with the SeaMARC II bathymetric sidescan sonar system during a survey of Fieberling Guyot [15], a massive structure rising from about 4500 m depth to 500 m below the sea surface in the northeastern Pacific (32°.5N, 128°W). In its normal mode of operation the sonar is usually towed at about 8–9 knots. It transmits a 1-ms pulse of 11 kHz on port and 12 kHz on starboard, and the seafloor echoes received are displayed to create an image whose width corresponds to a swath about 10 km wide.

Fig. 2(a) shows such an image from the above survey. Although this image is close to its raw form, time varying gain and manual gain changes have been corrected according to an algorithm described in [7] and the contrast has been slightly enhanced for ease of readability. The central line corresponds to the survey track going from top to bottom. This image contains most of the artifacts previously mentioned: the narrow lines running along-track on either side of the central gap result from a sea surface reflection of the near-nadir bottom returns; A consistent along-track nonuniform brightness is particularly obvious on the left side. The whole image is also very inhomogeneous when comparing adjacent pings. Finally, data have not been properly recorded during a few individual pings. This image is used in the following sections to verify and illustrate the performance of the various processing techniques described.

II. Prefiltering-Outliers Reduction

Our main goal is to improve the visual information content of backscatter images for interpretation purposes, by removing most of the noise components present in the image. As mentioned in the Introduction, certain forms of noise do more than simply mar the image, they also reduce the efficiency of subsequent linear processing schemes. A cursory examination

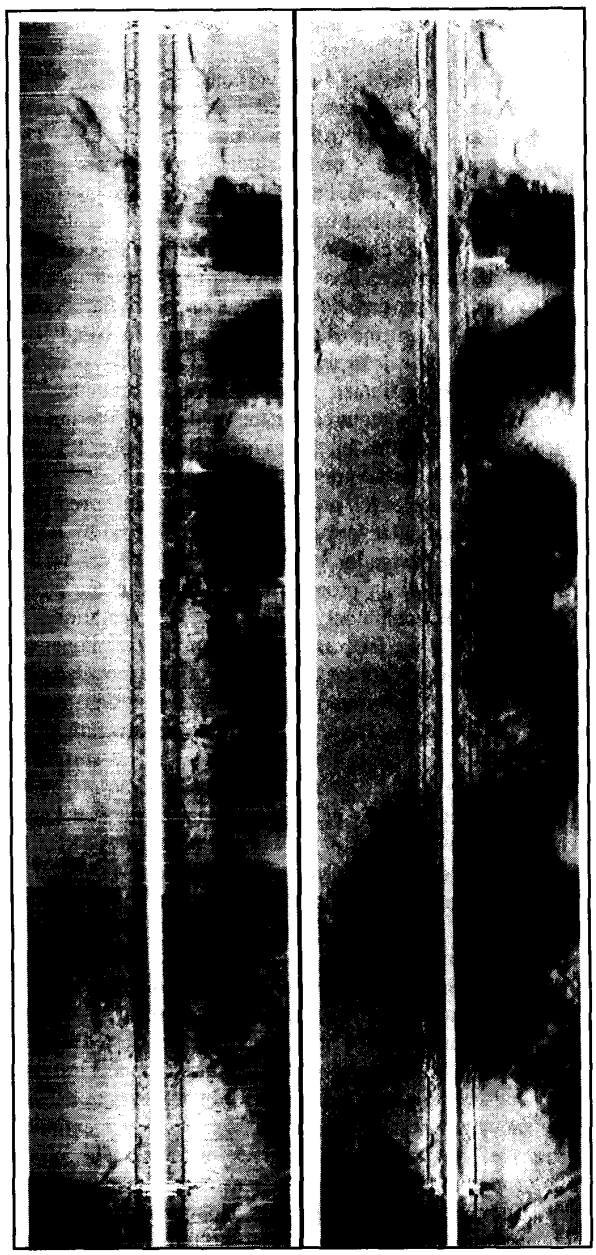

(a) (b)

Fig. 2. SeaMARCII sidescan images of the seafloor. Each image is displayed with a 10 km swath width. Navigation is not taken into account and a constant along-track step of 50 m is assumed between pings. Pixels are positioned across-track according to the "flat bottom" assumption. Strong echoes are dark. This and subsequent images have been printed on a Cannon high resolution laser color copier. Because of the printer's software and the available buffer memory space, the actual resolution is limited to 100 pixels/inch, and there are about 1000 points in a vertical line. (a) Original image after compensation for manual gain changes, plus contrast enhancement with a partial (50%) histogram equalization. (b) Processed image; gain correction, median+Chebyshev filters, systematic across-track correction, and contrast enhancement.

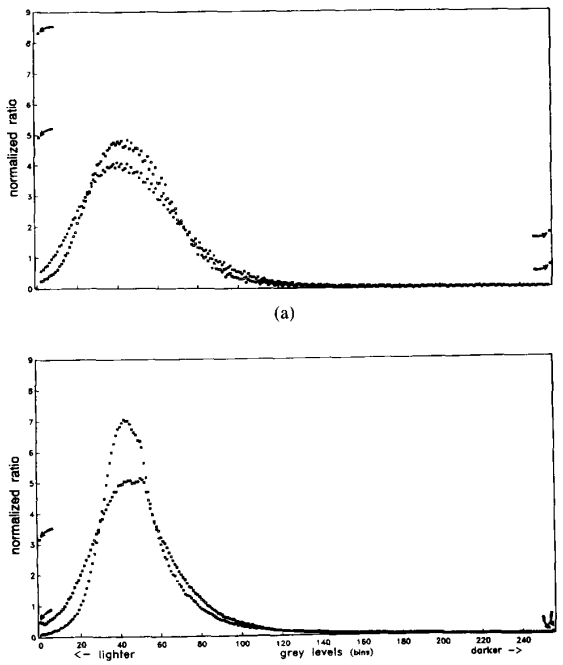

Fig. 3. Gray levels histograms for the left sides of Fig. 2(a) and (b) before contrast enhancement. Data are quantized with 8 bits, i.e., 256 levels. The ordinate axis is scaled so that a flat histogram is leveled at unity. Arrows point to low and high clipped levels. (a) Effect of median filtering alone. Filled squares: initial gain corrected image; empty squares: after median filtering. (b) Effect of Chebyshev filtering and systematic across-track correction, with (filled squares) and without (empty squares) intermediate median filtering.

of the gray-level histogram (Fig. 3(a), filled squares) for the left side of the original gain corrected version of our test image, shown contrast enhanced in Fig. 2(a), indicates a smoothly varying function with discontinuities at both ends. These discontinuities represent an amount of outliers, defined here as the number of pixels in the lowest and highest bins, departing from the levels found in their quasi-continuous neighborhoods. Counted as a percentage of the total number of pixels in the image, there are about 3% of low clipped values, and 0.7% in the high range for this example. Missing data (nulls) or saturated records (255's) are included in these proportions, but for the most part, these outliers are reminiscent of speckle noise [16].

Straightforward and well-known nonlinear methods such as median filtering are effective against outliers [13], [14]. The main advantage of median filters is their ability to remove outliers without blurring the edges of features present in the image because no averaging is performed. However, in dealing with GLORIA sidescan sonar images of the seafloor, Chavez [1] reports good speckle removal performance with a linear filter, by setting outliers to zero and by applying a small low-pass spatial filter (e.g., 2×2 or 3×3 averaging window), replacing all the zeros with the average of their nonzero neighbors delimited by the filter, and leaving all nonzero values alone.

Whether using a linear or nonlinear filter, care should be taken to consider the typically uneven along- versus across-track character of sidescan sonar images of the seafloor,

as opposed to conventional images for which approximately uniform 2-D sampling is assumed, allowing direct use of $N \times N$ filters.

To reduce noise spikes in sidescan sonar images, it is natural to think of applying the filtering process on data as they are recorded, i.e., across-track. In general such a process is very innocuous, because data are usually oversampled athwartships and then decimated to some degree before display on a monitor screen or printed on paper. For example, in the SeaMARC II data presented here, the across-track spatial sampling is designed to produce one pixel every 5-m horizontally, but the resolution is much lower at the scales typically used to display such data (about 1/200000 here). Thus, applying a short range (e.g., 3 points $\equiv$ 15 m) median filter across-track is very safe in terms of information content, as well as very efficient in reducing the amount of spikes in the image. For reference, the theoretical slant range resolution, which is approximately $c/2\omega$ with the speed of sound in seawater c in m/s and the bandwidth of the sonar system ω in Hertz, is 0.75 m for the SeaMARC II system when operated with a 1-kHz bandwith.

On the other hand, median filtering in the across-track direction does not improve saturated or null segments that are longer than the width of the filter. Such artifacts appear as black lines running across-track in Fig. 2(a). The linear filter described in the next section can greatly smooth these visual discontinuities. However, sole reliance on this linear filter is likely to result in alterations of the average absolute gray level in the entire neighborhood of such lines. Here again, nonlinear prefiltering provides the best guard against this side effect thus warranting the application of median filtering along-track.

The width of this along-track filter is set in relation to the along-track spatial sampling interval that is dictated by a combination of tow speed and ping rate, itself a function of the speed of sound and the water depth. Consequently, the spatial sampling interval is usually much larger along-track than across-track, where it is dictated by the signal bandwidth. In the case of SeaMARC II, there is an average of 40 m between pings under normal operating conditions (8 knots, 10-s ping rate).

Nonetheless, systematic along-track median filtering may induce significant perturbations in the original information content of the image, particularly if data are somewhat misregistered from one ping to the next due to errors in the first bottom detection. Keeping in mind that the purpose of this step is only to reduce the impact of very few bad records on the subsequent processing, we have adapted a simple thresholding scheme often used in exploratory data analysis [17] to isolate and modify only the outliers. Along-track substitution of pixel values under a 3-point median filter only occurs if the difference between the original value and its two neighbors exceeds a given minimum threshold. This parameter is chosen empirically (e.g., 50 for 256 gray levels), according to the average tone and contrast of the image. As a result, the along-track filter leaves most of the image unchanged, but it is able to limit by substitution the extent and amount of records that carry no information.

After application of these across- and along-track median filters, the shape of the gray-level histogram has changed somewhat (Fig. 3(a), empty squares) and the amount of outliers has decreased by about 50%. However, besides the obvious disappearance of a few black lines in the image, the immediate visual effect of this pre-filtering is hardly noticeable (Fig. 4(a)). But the effect on subsequent linear filtering processes is most important. Anticipating the results of the next section, Fig. 3(b) compares the histograms obtained after spectral processing with (filled squares) and without (empty squares) median prefiltering. In this example, without prefiltering, the linear process reduces the percentage of clipped pixel values from 3% to 1%, whereas median prefiltering brings the percentage from 3% to 1.8% and the subsequent linear processing reduces this number to 0.15%, for a 7-fold improvement in low clipped values rejection. Moreover, the histogram is much sharper when the nonlinear prefilter is applied, implying that the initial width of the histogram is partially enlarged by the presence of noise that the median filters reduce. Thus, the nonlinear preprocessing allows discrimination of the actual information content that emerges through the compact histogram of the image after the spectral analysis. In turn, at the final stage of the image processing, contrast enhancement algorithms (e.g., histogram equalization) have more latitude to stretch the gray levels, thus enabling amplification of image details and providing more satisfactory results.

III. Spectral Analysis

3.1. Theory

It is assumed that each processed image covers an area of seafloor whose acoustic backscattering properties remain relatively homogeneous. In other words, any portion taken within each rectangular frame, whose characteristic size is on the order of half a swath width, features the same type of bottom. With a shallow-towed sidescan sonar system such as SeaMARC II, this requires that the relief fluctuations be at least an order of magnitude smaller than the local water depth. In this section, we are looking at correcting variations of intensity by means of a linear filter. Therefore, it is now assumed that saturated or null values do not appear in large concentration.

Because sidescan sonars gather information on a ping by ping basis, the backscatter images are made of contiguous across-track line segments, with each segment constituting a quasi-continuous element of information. Consequently, to correct the erratic signal amplitude variations between adjacent pings we make a 1-D spectral analysis of each line (ping); then the spectral components are processed in the perpendicular direction (along-track).

The yaw of the fish adds low spatial frequency noise components in the across-track signal spectra. Hence, the low-frequency content of the recorded signal reflects partly the very nature of the seafloor and partly the artifacts introduced by the sonar's motion. However, unless the seafloor is very anisotropic, the fast along-track evolution of these components is mostly the signature of the artifacts. Thus, an along-track low-pass filtering of the very low spatial frequency components should not remove any seafloor information, but correct the artificial short range fluctuations.

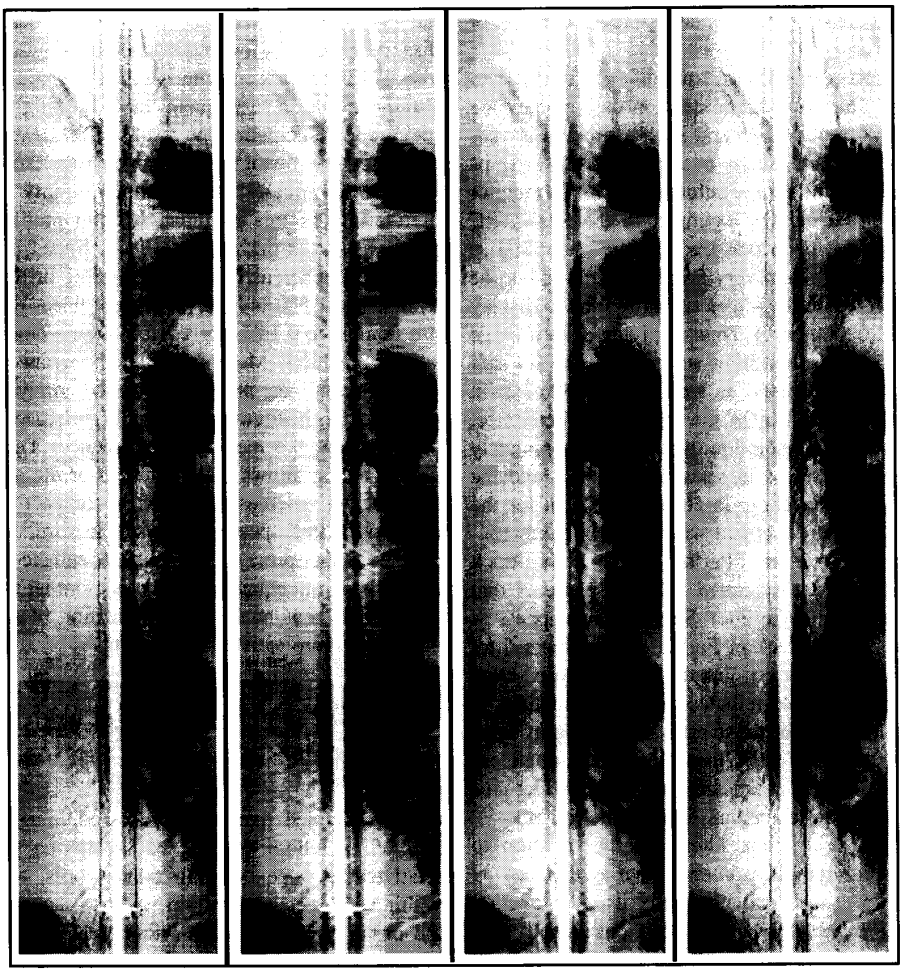

(a) (b) (c) (d)

Fig. 4. Linear image processing. (a) Gain corrected, median filtered image (initial image for this process). (b) Chebyshev approximation of (a). (c) Filtered version of (b). (d) Corrected image, i.e., (a) − (b) + (c). The systematic across-track correction is not included.

The same spectral analysis is also performed in the along-track direction over a number of pings stacked into a single record. We assume that the seafloor does not feature an anisotropy that would lead to significant along-track averages of the low-frequency coefficients. Accordingly, the residual content is attributed to artifacts that are removed over the entire frame. However, before performing this operation, the averaged coefficients are tapered to reduce the impact of the filter on the "higher" frequencies. This precaution must be taken to ensure that artificial features are not introduced. For example, as explained in Section 3.3, surface reflected echoes can appear as a narrow line running along-track. If this line undergoes small lateral fluctuations, a nontapered correction would introduce ghost images of this line over the whole frame. "Natural" narrow features could also introduce such artifacts. Avoiding this drawback is the main advantage of the spectral analysis compared to the direct approach: a conventional method that involves 1) stacking the backscatter amplitudes along track and 2) assuming the resulting across-track distribution is statistically uniform, performing a suitable correction over the whole frame (e.g., [1], [3], [4]). Our method is basically similar, but it limits the assumption of uniformity to the weighted low spatial frequency components.

For similar noise reduction applications to GLORIA sidescan sonar data, Chavez [1] used a combination of high-pass and low-pass $N \times M$ spatial filters to remove across-track striping in the images. Each filter was applied independently and the final image was obtained by summing their output. This technique has also been used with SeaMARC II data [4], but the anamorphic nature of most sidescan sonar images of the seafloor, as recorded in real-time, leads us to surmise that 2-D spatial filters are not necessarily appropriate.

With these general guidelines, one can think of decomposing the framed image into a set of basis functions. In choosing these functions, the concept of "low" or "high" spatial frequencies is related to the intuitive notion implied by the number

of median value crossings, or the number of sign changes of the second derivative, that characterize the corresponding basis function over a range of abscissa commensurate with the swath width.

Let us denote $s_y(x)$ the yth record in the sequence of pings making up the image, with the horizontal range x defined over the interval $[x_{\min}, x_{\max}]$. Assuming these records can be expressed as a linear combination of orthogonal functions $F_j(x)$, ordered in the sense of the spatial frequencies mentioned previously:

$$s_y(x) = \sum_{j=0}^{\infty} a_j[y] F_j(x) \tag{1}$$

it is possible to compute Fourier coefficients defined by

$$a_j[y] = \left(\int_{x_{\min}}^{x_{\max}} w(x) F_j^2(x)\, dx \right)^{-1} \int_{x_{\min}}^{x_{\max}} w(x) s_y(x) F_j(x)\, dx \tag{2}$$

where w is the weight factor that is associated with the orthogonal property of the family $\{F_j\}$ [18]. Note that in these equations and throughout this paper, we use parentheses ( ) for functions of a variable and square brackets [ ] for integer indexes.

The functions F_j need to be orthogonal for filtering operations to make sense as, in that case, the values of each component do not depend on the total number of functions kept to perform the decomposition. Hence, each spectral value can be obtained independently and easily by computing the corresponding Fourier coefficient.

The system of orthogonal functions we chose for this decomposition is the set of Chebyshev polynomials $T_n(x)$:

$$T_n(x) = \cos(n \arccos x) \tag{3}$$

with the first members of the set given by:

$$T_0(x) = 1,\ T_1(x) = x,\ T_2(x) = 2x^2 - 1. \tag{4}$$

These polynomials are orthogonal in the interval $[-1, 1]$ with a weight factor $w(x) = (1 - x^2)^{-1/2}$. This weight factor gives the necessary emphasis on both ends of the bounded function that we want to approximate, so that there is no "leakage" of accuracy at the edges. Chebyshev polynomials come very close to the minimax principle: The difference between the Chebyshev approximation and the initial function is spread evenly over the interval of definition ("equal-ripple"). Thorough discussions of these properties are found in many textbooks. The reader can refer to Hamming [18] for a user's perspective.

An important practical advantage of the Chebyshev set of functions is that the continuous interval in which they are defined can be replaced by a discrete set of samples over which the Chebyshev polynomials are also orthogonal. To this end, the continuous functions $T_n(x)$ are sampled into a set of discrete functions $T_j[X_i]$ that are orthogonal over two sets of abscissa equally spaced in angle θ. We use the set $\{X_i\}$ written over M sample points as

$$X_i = \cos(\theta_i), \quad \text{with} \quad \theta_i = \frac{i - 1/2}{M}\pi, \qquad i = 1, \ldots, M. \tag{5}$$

The uneven spacing of the points in X_i compensates for the weight factor $w(x)$ in (2). Hence, the backscattered amplitude profiles are resampled, by interpolations and/or decimations, over M locations $\{x_i\}$ according to

$$x_i = 1/2[(x_{\max} + x_{\min}) + X_i(x_{\max} - x_{\min})] \tag{6}$$

in which the dimensionless abscissae X_i are derived from (5). In addition, each Chebyshev polynomial takes the simple trigonometric form:

$$T_n(X_i) = \cos(n\theta_i) \tag{7}$$

so that the Fourier coefficients (2) are calculated directly with the following sums:

$$a_j[y] = \frac{2}{M} \sum_{i=1}^{M} s_y(x_i) \cos(j\theta_i). \tag{8}$$

Using the Chebyshev set, (1) becomes a polynomial expansion:

$$s_y(x) = \frac{a_0[y]}{2} + \sum_{j=1}^{\infty} a_j[y] T_j(X) \tag{9}$$

where $a_0/2$ is used for convenience. In practice, we compute an estimate $\sigma_y(x)$ of $s_y(x)$ by carrying the expansion of (9) up to order to order $(N - 1)$:

$$\sigma_y(x) = \frac{a_0[y]}{2} + \sum_{j=1}^{N-1} a_j[y] T_j(X) \tag{10}$$

where x and X are related by the continuous counterpart of (6).

3.2. Processing

To implement the spectral filter, we compute two sets of Fourier coefficients using (8). The first is a complete mapping $\{a_j[y]\}$ of N values per ping (and per side). The second set $\{a'_j\}$ of N' elements is calculated by replacing s in (8) with the single cumulated function:

$$f(x) = \frac{1}{Y} \sum_{y} s_y(x) \qquad (Y = \text{total number of pings}). \tag{11}$$

In practice, N' is usually greater than N. The coefficients a'_j with order $j \leq N$ are the along-track average of their counterpart in the set $\{a_j[y]\}$.

Both sets are then filtered to give respectively the new sets $\{\overline{a}_j[y]\}$ and $\{\overline{a'_j}\}$. Set $\{\overline{a'_j}\}$ provides a systematic correction:

$$c'(x) = \sum_{j=1}^{N'-1} \overline{a'_j} T_j(X) \tag{12}$$

in which the coefficient of order 0 is not taken into account to avoid altering the absolute levels. Set $\{\overline{a}_j[y]\}$ is used to replace the original spectral content of each record by its filtered version. For this, one evaluates

$$c_y(x) = 1/2(\overline{a}_0[y] - a_0[y]) + \sum_{j=1}^{N-1} (\overline{a}_j[y] - a_j[y]) T_j(X). \tag{13}$$

The corrected image is then obtained by removing the difference between the systematic correction and the filtered correction from the original image:

$$\bar{s}_y = s_y(x) + c_y(x) - c'(x). \tag{14}$$

Implementation of these filters must be done very carefully in order to avoid removing "true" seafloor features. For the systematic correction, we apply a parabolic taper on each coefficient a'_j:

$$\overline{a'_j} = \left(1 - \left[\frac{j-1}{N'-1}\right]^2\right) a'_j, \qquad 1 \le j < N' \tag{15}$$

so that the first order component a'_1, i.e., the average gray level slope, is completely removed from the image ($\overline{a'_1} = \bar{a}_1$), whereas the higher average components are decreasingly weighted, up to orders N' and higher that are left unchanged by the systematic correction. In selecting N', one must keep in mind that the higher the degree of the corresponding polynomial, the smaller the size of the across-track features that are likely to be altered, or even introduced when things go wrong (along-track stripes). In our algorithm, N' is an adjustable parameter, but several tests showed that values around a few tens usually give satisfactory results with a parabolic window.

The y-filtering of the set $\{a_j[y]\}$ must cope first with occasional missing data that the prefiltering described in Section II has been unable to handle. Missing data are usually associated with "bad" pings and they introduce outliers in the series $\{a_j[y]\}$. As discussed in Section II, preprocessing the series with a 3-point median filter provides a simple and effective solution to this problem. Then, a low-pass convolution is performed to smooth the local variations occurring between adjacent pings, for each component a_j. This is achieved by windows $b_j[y]$ whose area is unity:

$$\bar{a}_j[y] = a_j[y]^* b_j[y], \qquad 0 \le j < N \tag{16}$$

where * denotes the convolution operation.

We chose parabolic tapers with $p = 2q + 1$ points for the window $b[y]$:

$$b[y] = \frac{6}{p(p+1)(p+2)}[(q+1)^2 - y^2], \qquad -q \le y \le q. \tag{17}$$

For a given order j of the filtered component $\bar{a}_j$, the size p of the window b_j is constrained by the fact that the spatial wavelength of each mode is directly referenced to the swath width. With such a window, the same amount of along-track smoothing is less likely to remove slowly changing geomorphologic features than other patterns evolving rapidly along a short range of pings. As the minimum effective (odd) width of a window is $p = 3$, we define a function $p[j]$ in terms of the maximum number N of processed components through:

$$p[j] = 2[(N-1)\%j] + 1, \qquad 1 \le j < N \tag{18}$$

where the symbol % stands for the arithmetic division.

Therefore, the window width is inversely proportional to j in the same way the spatial wavelength is inversely proportional to the component's order. As a result, the pertinent parameter is the number of filtered orders, N, which we link with the ratio between the width of the image, and the along-track ping spacing, Δy, by

$$N = A\left[\frac{x_{\max} - x_{\min}}{\Delta y}\right]^{1/2} \tag{19}$$

in which A is an adjustable parameter, whose order of magnitude is unity. Doing so, the highest filtered order is convolved by a window whose length has the same order of magnitude as the across-track size of the smallest feature represented by this component, i.e., the approximate length of the narrowest ripples of function T_N calculated with $|X|$ close to unity in (7).

Another specific treatment can be applied on the 0th-order component. Instead of evaluating $\bar{a}_0[y]$ through the convolution given in (16), it can be reset for every ping, y, to a constant value, e.g., the medium gray level. This is useful for processing images in which manual gain changes have not been corrected. An example of this feature is presented in Section 3.3.

3.3. Application

Fig. 4(a) displays the image as it enters the spectral process. As in Fig. 2(a), it has been corrected for manual gain changes, but it is not contrast enhanced. Median pre-filters have been applied. The Chebyshev approximation, $\sigma_y(x)$ (10) with $N = 22$ components, is shown Fig. 4(b). Most of the obvious artifacts that we want to remove are found in this representation. Fig. 4(c) exhibits the smoothed Chebyshev approximation, $\bar{\sigma}_y(x)$, computed with (10) where the coefficients a_j are replaced by their filtered versions, $\bar{a}_j$. The higher order components present in the difference between Fig. 4(a) and Fig. 4(b) are added back to this filtered approximation to produce Fig. 4(d). Note that Fig. 4(d) is a partial representation of (14) as the systematic along-track correction term, $c'(x)$, is not included.

As mentioned previously, the number of filtered orders, N, is dictated by the along-track resolution compared to the across-track width of the image. Filtering noise is always a matter of balance with altering "true" information content. Whenever fine details seem to be missing in the filtered image, the maximal Chebyshev order can be decreased. Previous tests, performed with $N = 7$ on the same image, yielded a noticeable improvement in the image appearance [19]. This implies that the defects we tried to remove affect only the very low modes, and that, if properly applied, this correction will most likely preserve the seafloor echo signatures that the end-users want to analyze.

Results of the along-track processing are shown in Fig. 5, where the solid line represents the average across-track profile (11) for the right side of Fig. 4(a), and the dotted line represents the systematic correction based on the Chebyshev filtering ((12), (15)), with $N' = 30$. Once this averaged, smoothed profile is subtracted from each ping in the image shown in Fig. 4(d), and after a slight contrast enhancement, we get the result displayed in Fig. 2(b) that must be compared with the original image of Fig. 2(a).

From a practical point of view, Chebyshev analysis is not difficult to perform. The computation of the Fourier coefficients with (8), and the correction mapping with (13)

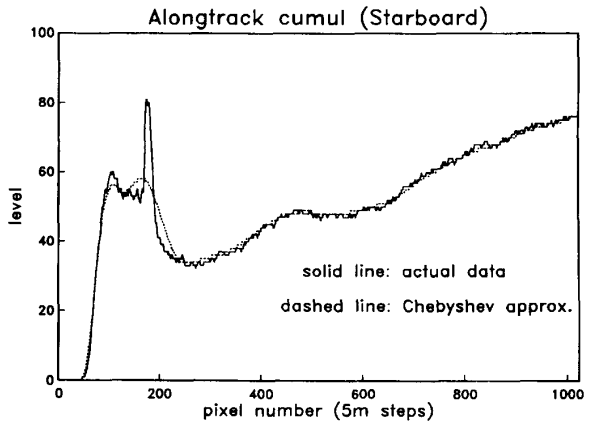

Fig. 5. Systematic across-track correction. Solid line: Actual across-track profiles averaged along-track; dashed line: Chebyshev approximation used to perform the correction.

use several samplings of cosine functions that only need to be evaluated once and are then stored for all subsequent pings. Equation (12) is also computed only once.

As mentioned in Section 3.2, this filtering technique has the advantage of being impervious to changes in gain settings made by watch-standers during data acquisition at sea. This point is best illustrated with the raw image (Fig. 6(a)) that we have used to test the processing techniques described in this paper. Several manual gain changes are visible in this image: seven on the right side, and three on the left. Processing these raw data without any *a priori* knowledge of the gain settings, i.e., assigning $\overline{a}_0 = 128$ in (13), and performing contrast enhancement, yields the image shown in Fig. 6(b) to be compared with that of Fig. 2(b) where gain changes have been taken into account before filtering. The net effect is to center the gray-level histogram on the median level (128), as shown in Fig. 7 (filled triangles). An obvious side effect of this solution is loss of information about the actual levels of seafloor acoustic backscatter recorded, and a potential increase in amplitude clipping because the original histogram is shifted.

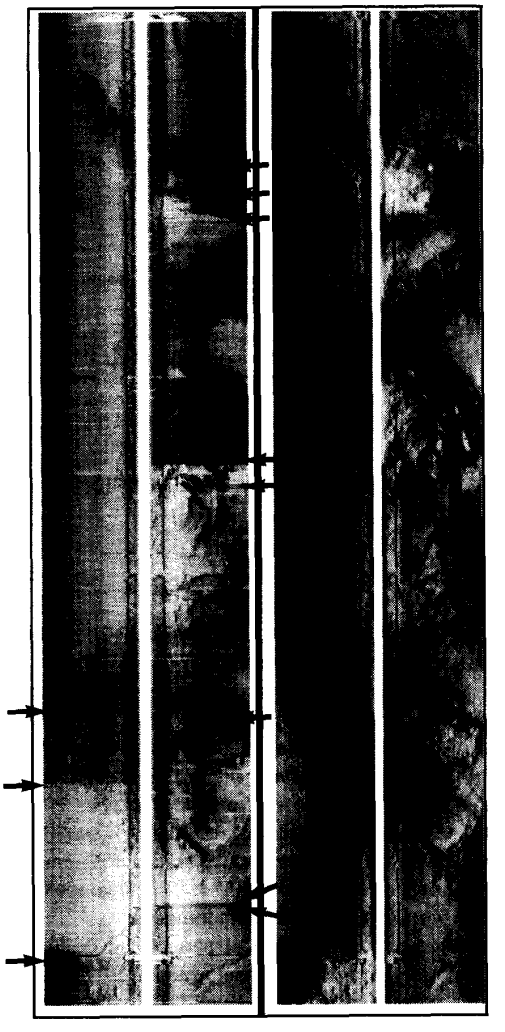

(a) (b)

Fig. 6. Raw and processed sidescan images. (a) Original image. Arrows indicate when manual gain changes occur. (b) Result of median filtering, Chebyshev filtering (with zeroth order reset at medium gray level), systematic across-track correction, and contrast enhancement.

IV. Histogram Equalization for a Complete Survey

A seafloor imaging survey with sidescan sonars generally consists of several adjacent swaths run along more or less straight courses. When assembling all these swaths into a map, it is desirable to provide a common reference for the recorded levels of seafloor acoustic backscatter throughout the survey area and to preserve the relative backscattering contrast of geological features while improving the overall appearance of the image for interpretation. This is normally done with conventional image contrast enhancement techniques applied locally or globally (e.g., [7]). From a practical point of view, given that our image segments are processed in a rectangular format with the techniques described in Sections II and III, it is easier to undertake the contrast enhancement in this format and prior to navigation corrections that tend to introduce gaps along track.

One of the simplest classical methods to achieve contrast enhancement is the histogram equalization technique [20]–[22]. It is a single valued transform, designed to produce a uniform distribution of pixels per gray level.

Given a gray scale quantized to (u) levels, the histogram $h[i]$, $i = 0. n - 1$ of the image is scaled such that:

$$\sum_{i=0}^{n-1} h[i] = 1. \tag{20}$$

With this representation, each gray level u is transformed into a gray level v according to a single-valued monotonic law. The corresponding transform can be implemented in a number of ways, each leading to slightly different results. We chose an ascending scheme with a transform $v[u]$ that overcomes

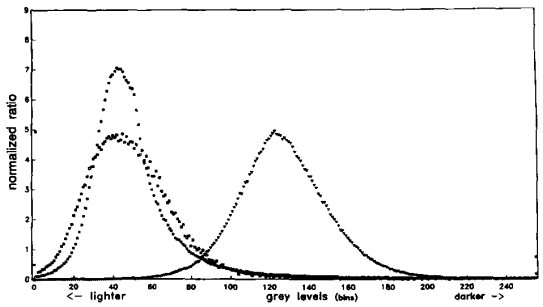

Fig. 7. Effect of Chebyshev filtering on gray-level histograms. Empty squares: Initial gain corrected and median filtered image (Fig. 4(a)). Filled squares: image after Chebyshev filtering and systematic across-track correction (Fig. 8(a)). Filled triangles: Chebyshev filtering and systematic across-track correction, with zeroth-order reset at medium gray level (Fig. 6(b)).

boundary problems and keeps outliers unchanged:

$$v[0] = 0,\ v[n-1] = n-1, \quad \text{and}$$
$$v[u] = (\text{int})\left[n \sum_{i=0}^{u} h[i]\right], \qquad u = 1, \ldots, n-2. \quad (21)$$

As a consequence of the data digitization, the total number of levels that are actually assigned by (21) is less than n. Several bins in the new histogram are empty, and the distorted shape of the original histogram can still be seen. However, provided the number of gray levels in the original image is large enough, this artifact has no visual impact on the image, as can be verified by decimating the sparse histogram. For the specific case of sidescan sonar images of the seafloor, another way to illustrate this is to convolve each record across-track with a short, 3-point window (1/4, 1/2, 1/4): the image looks exactly the same, but the histogram is smoothed flat.

If the average tone of a small part of the original image is very different from that of the whole area, details in this part of the image can be lost through the equalization process which moves the level of the corresponding pixels toward an extremity of the histogram. Hence, it is useful to be able to adjust the efficiency of the transform by altering the shift of each gray level ($v[u] - u$ derived from (21)) with a linear coefficient, α:

$$v[0] = 0,\ v[n-1] = n-1, \quad \text{and}$$
$$v[u] = (\text{int})\left(u + \alpha\left[n \sum_{i=0}^{u} h[i] - u\right]\right),$$
$$u = 1, \cdots, n-2. \quad (22)$$

The image remains unchanged for $\alpha = 0$ (Fig. 8(a), and $\alpha = 1$ yields the original equalization transform (Fig. 8(c)). Values of α in the interval [0, 1] yield intermediate results as seen in Fig. 8(b) for $\alpha = 0.5$. The coefficient α is normally kept in this interval so as to preserve the original order of gray levels through the transformation of (22):

$$u1 < u2 \Rightarrow v[u1] \leq v[u2]. \quad (23)$$

However, if we use an unusually large coefficient, $|\alpha| \gg 1$, and appropriately clip the transform of (22) for over- and under-flows, it is possible to map the translation direction of each pixel's gray level. The resulting image contains mostly black and white areas, although some pixels will retain their original gray level.

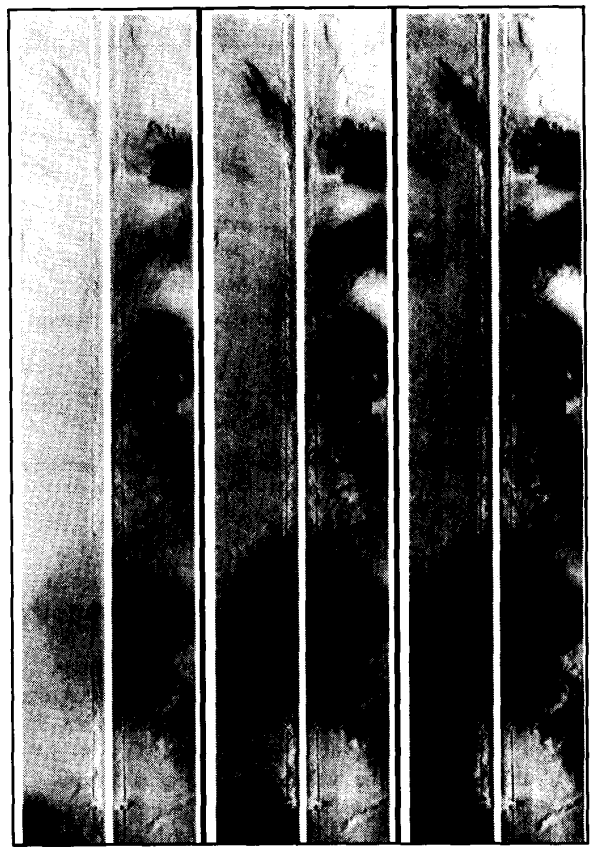

(a) (b) (c)

Fig. 8. Effect of histogram equalization on a filtered image: (a) no contrast enhancement, (b) 50% histogram equalization (same as Fig. 2-b), (c) 100% histogram equalization.

With this basic equalization scheme, a global gray level histogram for the entire survey area is built. To this end, we assume that there are few overlapping areas in the survey or, if such is not the case, that data segments have been chosen to minimize overlaps. Then, the global histogram h is the weighted sum of the histograms of the individual segments, h_j, normalized according to (20):

$$h[i] = \frac{1}{\sum_j p_j} \sum_j p_j h_j[i] \quad (24)$$

where p_j denotes the number of pixels in the jth segment.

This is similar to the global equalization method, called "age processing scheme" by its users (e.g., [7]), that preserves a common reference for the relative acoustic backscatter levels recorded over the area. A relative "age" can be inferred from such maps of midocean ridges and adjacent areas, by associating high backscatter levels with younger crust or bare rock and lower levels with older crust covered with sediments of varying thicknesses. Depending on the geology of the area

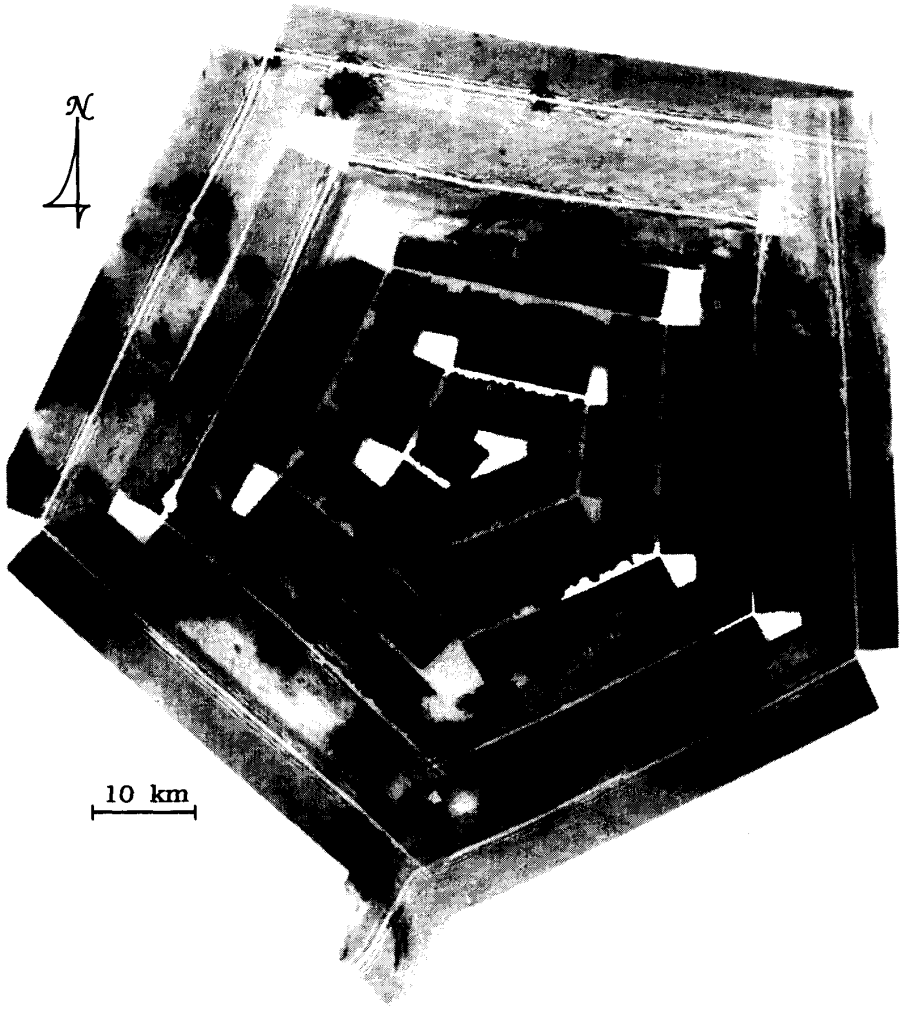

(a)

Fig. 9. Contrast enhancement by histogram equalization (complete view of Fieberling Guyot). (a) Using the global histogram only.

surveyed, and for the same reasons that led to the introduction of a coefficient α in (22), a transform such as (21) based directly on the global histogram will likely render certain areas of the survey overly dark or light, hence masking details. Although this problem is overcome by using the same technique, only limited contrast enhancement may be achieved for each segment.

In order to highlight details everywhere in the survey mosaic, others have used a "structure" processing scheme (e.g., [4], [7]) whereby histogram equalization is performed independently on each segment or sub-area of the survey data. Although this method is very effective in bringing out the structural characteristics of the seafloor surveyed, its main side effect is loss of the relative brightness between the different segments considered in the map, because individual histograms have been centered on their respective median. To alleviate this side effect, we chose a compromise solution in which each individual segment is processed with a reference histogram, h'_j, made of a linear combination of the global histogram, h, and the histogram, h_j, of the segment considered:

$$h'_j[i] = (1 - \beta)h[i] + \beta h_j[i]. \tag{25}$$

The coefficient β is chosen for the whole survey to balance the respective influence of the global and local histograms. Note that the final transforms can also take advantage of the weighting factor α, so that the gray level changes can be calculated with (22) in which $h[i]$ is replaced by $h'_j[i]$ given in (25).

Equalization calculated with such histograms has two interesting properties, both based on linearity: 1) within a homogeneous portion of the survey, the transform is independent of the size of the sub-areas resulting from the splicing

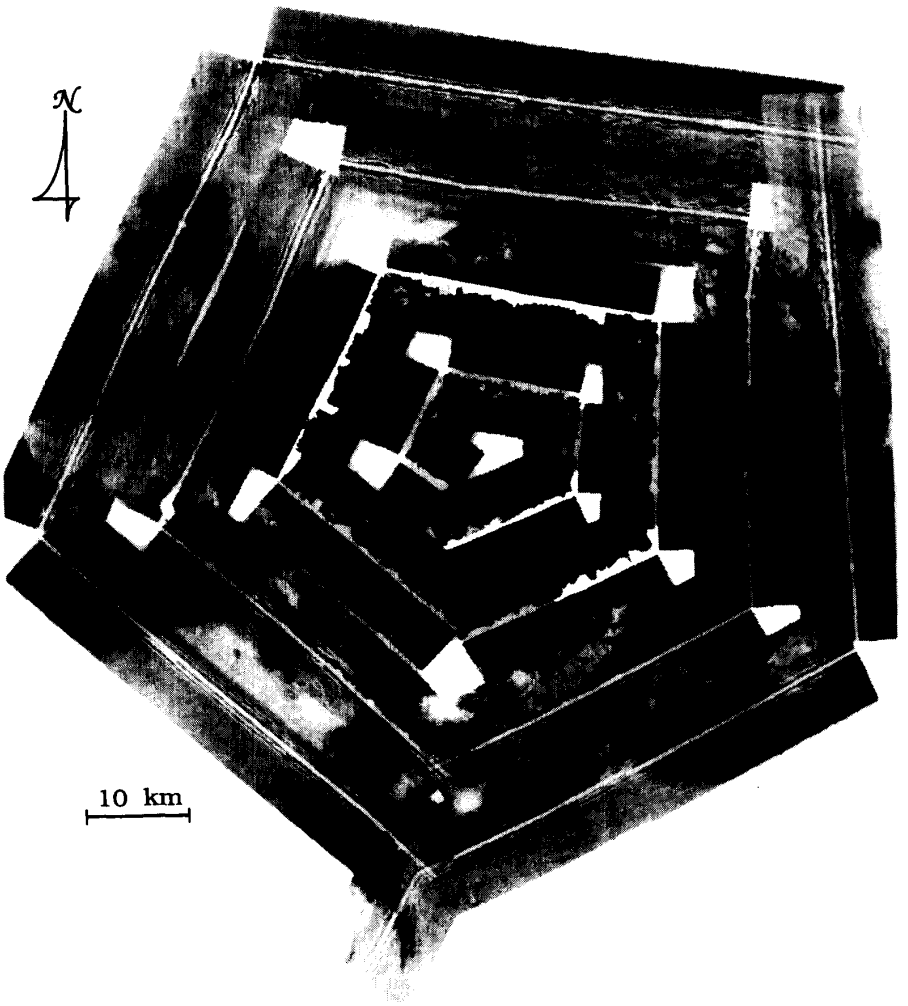

(b)

Fig. 9. Contrast enhancement by histogram equalization (complete view of Fieberling Guyot). (b) Using a balance between global and local histograms (with $\beta = 0.5$ in (25)).

process; 2) regardless of the value of coefficient β, the global histogram for the new image mosaic is "flat," except for the empty bins resulting from digitization. We have obtained satisfactory results with $\beta = 0.5$.

We have applied this technique to SeaMARC II sidescan sonar imagery collected over Fieberling Guyot [15]. Data segmentation followed the pentagonal pattern of the survey with boundaries set to yield a minimum amount of overlap between swaths. Histogram equalization based on the global histogram (Fig. 9(a)) provides a starker contrast between high and low backscattering surfaces, than does the equalization balanced between local and global histograms (Fig. 9(b)). However, features are easier to visualize in the darker areas of the latter. Details of the mosaicing technique used for these figures are given in the next section.

V. Navigation Corrections and Mosaic

After the various filtering and contrast enhancement operations described above have been performed, the last stage of processing involves placing each pixel in a geographic reference frame to assemble a mosaic of the various survey segments considered. To this end, the acoustic backscatter

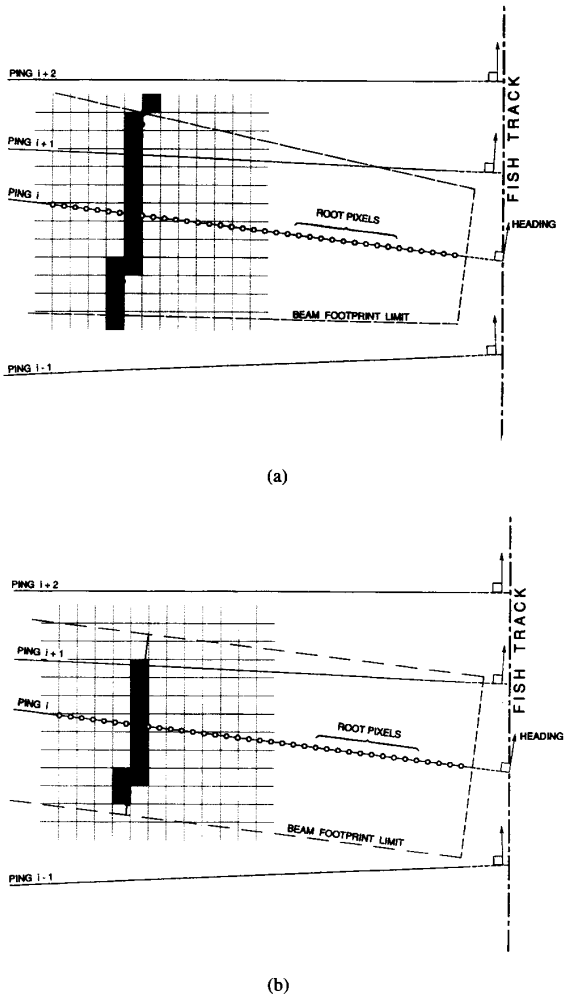

Fig. 10. Along-track filling process during transfer to geographic coordinates. (a) Filling scheme based on the beam footprint only, and (b) constant maximal along track extent and no overlapping beyond adjacent pings. In these figures, the relative scale of the beam footprint, the interval between pings, the spacing between adjacent bathymetry samples, and the pixel size bear no relation to actual physical scales and are for illustration purposes only.

data are merged with navigation data (time, latitude, longitude, and heading), in real-time during data acquisition or in post-processing by matching recording times. Pixels are then mapped from the rectangular frame used for filtering to a new rectangular grid of geographic coordinates computed according to standard map projections (e.g., UTM, Mercator, etc. [23]).

The choice of cell size for the geographic grid depends on the spatial resolution of the sonar data available. In the following we consider resolution in terms of how well the software can represent the original spatial characteristics of the data. Subsequent conversion from computer memory to a physical image will alter this resolution depending on the plotting device and its internal algorithm. For instance, the printer we use for gray scale, or color generation, maps a pixel in a cell of 4×4 dots.

In most cases, the across-track spatial sampling of the filtered rectangular frame for a single swath is regular, and it results from the projection of slant ranges to horizontal ranges based on a flat bottom assumption or on an instantaneous athwartships bathymetric profile measured with the system or created from a database. Assuming that, for each ping, pixels lie on the line of intersection between the vertical transmit plane and the seafloor, and that the coordinates of the sonar at the time of transmission are known. Then, it is straightforward to calculate a coordinate, at the desired projection, for each pixel of the original rectangular frame. However, depending on the resolution and scale of the geographic grid, there might be gaps between these remapped pixels. Between adjacent pings, such gaps form polygons that need to be filled before the image is displayed. Malinverno *et al.* [4] replace empty pixels within such polygons with values that are linear combinations of those pixels at the vertices of the polygon, weighted according to an inverse-square-distance law. This method is effective, but it can distort the shape of features along-track because it does not take into account the along-track spread of the beam footprint.

Due to the geometry of the measurement, the resolution cell of a sidescan sonar image covers an increasingly elongated area in the along-track direction, from nadir out. Hence, the smallest pixel size that is pertinent to define for the navigated image is dictated by the across-track sampling. The original across-track step defines the unit interval for computing theoretical locations in continuous coordinates. Reduced to discrete coordinates, these locations select the pixels for which a value is assigned. In practice, the pixel size for mosaics is chosen larger than the unit length. For example, SeaMARC II backscatter images of the seafloor are typically displayed with pixels at 20-m intervals across-track rather than the 5 m used at data acquisition time. As a result, successive data within a ping fill pixels that are contiguous or overlap, and there is no need to interpolate across-track. On the other hand, in order to avoid gaps along-track, values assigned across-track to these selected pixels must be spread along-track in proportion to the corresponding width of the beam footprint and to the horizontal distance travelled between pings.

As a first step in this along-track filling method, each original datum is spread with a triangular shading on a line parallel to the fish heading, over an extent commensurate with the beam footprint. The corresponding weights and weighted values are stacked in the cells that contain these theoretical locations (Fig. 10(a)). This yields an oversampled representation of the surveyed area, and the image is completely filled. Although it takes into account the fact that each datum carries information backscattered from elongated areas of the seafloor, a significant side-effect occurs for the same reason: the finite along track size of the acoustic beam footprint acts as a convolving window in probing the seafloor. So the above triangular window performs another convolution in the same direction, hence decreasing even more the along-track resolution and smearing geologic features along-track (Fig. 11(a)).

To lessen this effect, the maximal extent of the along-track spreading is computed as the lesser of the average distance travelled between pings and the beam footprint. In addition,

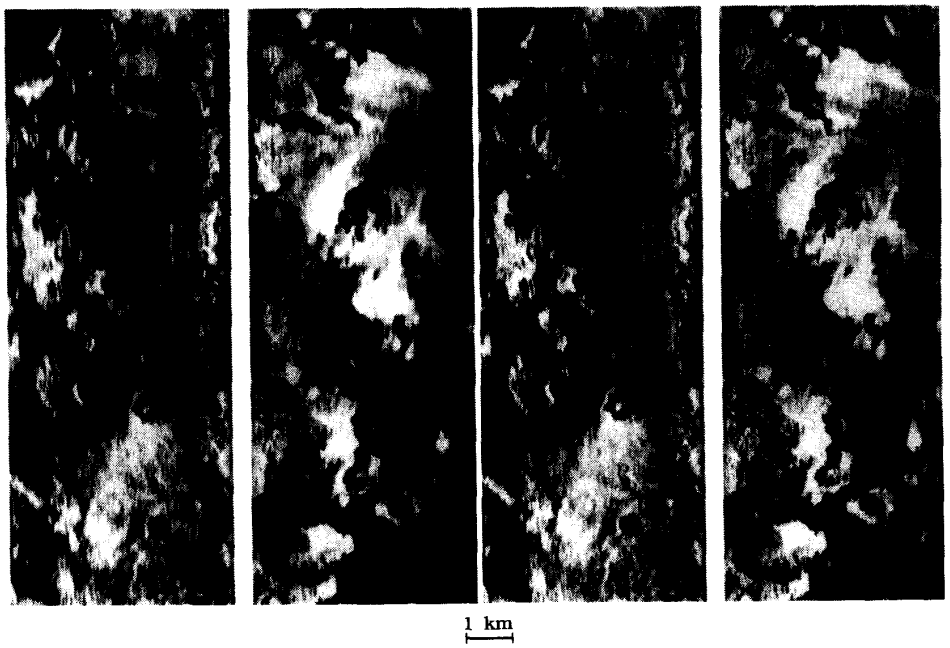

Fig. 11. Comparison of along-track filling procedures, according to (a) the scheme displayed Fig. 10(a); (b) the scheme displayed Fig. 10(b). These data were extracted from the flank of Fieberling Guyot, at midslope.

Fig. 12. Example of navigation correction applied to the data displayed in Fig. 8(b).

the stretched segments are limited by their first intersection with the closest "root" neighbors. Root pixels are defined as pixels lying on the line of intersection between the transmit vertical athwartships plane and the seafloor. To perform this remapping, the algorithm is conveniently built with two steps: a first pass assigns and stacks a value to one pixel per original datum. These "root" pixels are flagged by inverting the sign of the weight. Then, a second pass extends forward and backward the area of each datum, halting the painting process as soon as another pixel with a negative weight is reached (Fig. 10(b)). This method limits as much as possible the along-track spreading, while building a smooth transition between adjacent pings, hence improving the quality of large-scale images (Fig. 11(b)).

In our implementation, we generate three rectangular arrays whose number of elements is identical. An array is used to accumulate weighted pixel values, and a second array serves to stack the corresponding weights. The third array stores the image (8-bit values) resulting from the division of the first array by the second. Moreover, in order to save time when assembling mosaic images of surveyed areas, we found it more advantageous to produce first a set of large scale, navigated segments. Each rectangular frame is navigated and oriented according to the average course of the tow fish over that segment (e.g., Fig. 12). All such navigated files are saved as raster images (SUN format) with all the information needed to build mosaics inserted at the top of the image. This includes the scale, a reference point (that may include depth) given in both geographic and graphic coordinates, and the orientation of the image (heading). This way, images are readily displayed on a monitor or printed. Likewise, smaller scale mosaic images can be assembled expediently at any desired orientation with an iterative two-step process designed to save memory space. 1) Each individual image is rescaled

on a new grid at the orientation of the final mosaic. This operation is performed with triplicate arrays (stacked values, number of values, final division). 2) The mosaic image is built by transferring the previous temporary images, pixel by pixel, on a larger grid whose size increases at each iteration. At this stage, it is unusual to find regions with more than two overlapping layers. Consequently, it is no longer necessary to allocate the large amount of memory that a triplicate array scheme requires.

In areas of the mosaic where data overlap (in step 2 above), we have considered two simple options: 1) straight substitution of pixel values following the order in which they are loaded into the image grid, or 2) average the nonzero pixel values falling on the same grid point (option used to build Fig. 9). With the first option, to view the contribution of a particular segment in the overlapped region, one simply loads it after all the other underlying segments. More sophisticated schemes have been implemented (e.g., [1], [2]) however, in spite of the discontinuities it produces in the image, option 1) is probably the more realistic because what appears on a sidescan images of the seafloor is so dependent on the look angle. In addition, for systems like SeaMARC II different acoustic frequencies are used on each side, and one might have to normalize the data to a common reference before any kind of averaging scheme can be used on overlapped segments where both frequencies are involved.

VI. Conclusion

We have presented efficient implementable techniques to build sidescan sonar images of the seafloor from raw recorded data. Our goal was to provide the end-user with images displayed in a geographic reference frame with a minimum amount of artifacts and with improved contrast or feature definition, while retaining as much as possible the relative acoustic backscatter contrast due to the geology of the area.

Four main steps were used: 1) 3-point median prefiltering applied separately along and across-track to remove outliers; 2) spectral filtering that achieves most of the image enhancement, and only requires straightforward computations of a few coefficients per ping; 3) contrast enhancement with a modified gray-level equalization technique; and 4) mapping on a geographic grid that takes into account the point-spread function of the acoustic beam and the horizontal travel of the sonar between pings to minimize along-track smearing of features. Throughout this processing sequence, we employed algorithms that were designed to limit computation time and memory space requirements.

Admittedly, median filtering and histogram equalization techniques are well known in image processing applications. In this paper, we have attempted to provide a rationale for their use in sidescanned acoustic images of the seafloor whose data are inherently anamorphic and with recorded backscatter levels strongly dependent on the direction of insonification. For median filters, the emphasis was placed on the importance of their contribution to subsequent linear filtering operations. Likewise, the histogram equalization application stressed preservation of the relative brightness of the different parts of a survey mosaic, while providing sufficient contrast boost on a local level.

The linear filtering technique we have developed is purely stochastic and has the advantage of retaining the absolute amplitude levels of the echoes displayed. If the absolute values were not needed, the processing can also be set to correct for amplitude variations caused by manual gain changes, imparted during data acquisition at sea, without requiring *a priori* knowledge of these changes. A comparison of Fig. 2(a) and (b) underscores the benefits and limitations of the method. It brings out features in the final image that were difficult to see in the original. However, it does not remove strongly contrasted narrow artifacts, such as the surface multiple still apparent in Fig. 2(b), that require further specific processing. Also, in its current implementation, the original image must fit exactly in a rectangular frame for the method to work satisfactorily. This may create problems when processing backscatter images whose pixels have been remapped from a flat-bottom representation to an actual bathymetric profile yielding wavy boundaries.

Acknowledgment

We thank A. N. Shor for his support and Jo Griffith for the artwork.

References

[1] P. S. Chavez, "Processing techniques for digital sonar images from Gloria," *Photogrammetric Eng. and Remote Sensing*, vol. 52, pp. 1133–1145, 1986.

[2] J. M. Augustin, "Side scan acoustic images processing software," in *Proc. Working Symp. Oceanographic Data Systems*, pp. 221–228, 1986.

[3] T. B. Reed and D. M. Hussong, "Digital image processing techniques for enhancement and classification of SeaMARC II sidescan sonar imagery," *J. Geophys. Res.*, vol. 94, pp. 7469–7490, 1989.

[4] A. Malinverno, M. H. Edwards, and W. B. F. Ryan, "Processing of SeaMARC swath sonar data," *IEEE J. Oceanic Eng.*, vol. 15, pp. 14–23, 1990.

[5] D. T. Cobra, A. V. Oppenheim, and J. S. Jaffe, "Geometric distortions in sidescan sonar images: a procedure for their estimation and correction," *IEEE J. Oceanic Eng.*, vol. 17, pp. 252–268, 1992.

[6] R. C. Searle, T. P. LeBas, N. C. Mitchell, M. L. Somers, M. L. Parson, and Ph. Patriat, "GLORIA image processing: The state of the art," *Marine Geophys. Res.*, vol. 12, pp. 84–94, 1990.

[7] D. D. Bergersen, "A synopsis of SeaMARC II side-scan processing techniques," in *Proc. IEEE Oceans '91*, vol. 2, pp. 921–926, 1991.

[8] C. G. Fox, F. J. Jones, and T. K. Lau, "Constrained iterative deconvolution applied to SeaMARC I sidescan sonar imagery," *IEEE J. Oceanic Eng.*, vol. 15, pp. 24–31, 1990.

[9] D. C. Mason, T. P. LeBas, I. Sewell, and C. Angelikaki, "Deblurring of Gloria sidescan sonar images," *Marine Geophy. Res.*, vol. 14, pp. 125–136, 1992.

[10] J. A. Bangham, K. Y. Cheung, and R. Coates, "Processing of sidescan data using statistical filtering," in *Proc. IEEE Oceans '90*, pp. 57–62, 1990.

[11] P. Cervenka, C. de Moustier, and P. F. Lonsdale, "Correction of sidescan sonar images based on bathymetry. Application with SeaMARC II and SeaBeam data," *Marine Geophys. Res.*, submitted.

[12] J. G. Blackinton, "Bathymetric mapping with SeaMARC II: An elevation angle measuring side-scan sonar systems," Ph.D. dissertation, Univ. Hawaii at Manoa, 1986.

[13] N. C. Gallagher, Jr. and G. L. Wise, "A theoretical analysis of the properties of median filters," *IEEE Trans. Acoust., Speech, Signal Processing*, ASSP-29, pp. 1136–1141, 1981.

[14] B. I. Jutusson, "Median filtering statistical properties," in *2-D Digital Signal Processing Part II: Transforms and Median Filters*, Huang, T. S. Ed. New York: Springer-Verlag, 1981.

[15] C. de Moustier, P. F. Lonsdale, and A. N. Shor, "Simultaneous operation of the Sea Beam multibeam echo-sounder and the SeaMARC II

bathymetric sidescan sonar system," *IEEE J. Oceanic Eng.*, vol. 15, pp. 84–94, 1990.
[16] J. W. Goodman, "Statistical property of laser speckle patterns," in *Laser Speckle and Related Phenomena*, J. C. Dainty, Ed. New York: Springer-Verlag, pp. 9–75, 1975.
[17] J. W. Tukey, *Exploratory Data Analysis.* Reading, MA: Addison-Wesley, 1977.
[18] R. W. Hamming, *Numerical Methods for Scientists and Engineers.* New York: Dover Publications, 1973, chs. 25–29.
[19] P. Cervenka and C. de Moustier, "Sidescan sonar image enhancement using a decomposition based on orthogonal functions. Applications with Chebyshev polynomials," in *Proc. IEEE Oceans '91*, vol. 2, pp. 942–947, 1991.
[20] R. C. Gonzales and P. Wentz, *Digital Image Processing.* Reading, MA: Addison-Wesley, 1977.
[21] W. K. Pratt, *Digital Image Processing.* New York: Wiley, 1978.
[22] A. Rosenfeld, and A. C. Kack, *Digital Picture Processing*, vols. 1 and 2. New York: Academic, 1982.
[23] J. P. Snyder, Map projections used by the US Geological Survey, Washington, D.C., US Gov. Printing Office, 1982.

Pierre Cervenka received the Doctorate degrees in acoustics (1982) and physics (1988), both from the Universite de Pierre et Marie Curie, Paris.

In 1983, he joined the Centre National de la Recherche Scientifique (CNRS) as a research scientist. Most of his studies were involved with nonlinear acoustics and modeling of parametric antennae. From 1989 to 1992, he was a visiting assistant researcher at the Marine Physical Laboratory of the Scripps Institution of Oceanography. He is now with the Laboratoire de Mecanique Physique (Universite Paris 6), where his research interests are in underwater acoustics.

Christian deMoustier (M'86) received the Diploma of Engineer from the Ecole Superieure d'Ingenieurs de Marseille, France, in 1979, and the M.S. and Ph.D. degrees in oceanography (applied ocean science) at the University of California, San Diego, in 1981 and 1985, respectively.

He is with the Scripps Institution of Oceanography, where he is an Assistant Research Oceanographer at the Marine Physical Laboratory, and an Academic Administrator for Ship Operations and Marine Technical Support. His research interests are in underwater acoustics with emphasis on physics of bottom-interacting sound and sound reverberation in the ocean, seafloor acousitc imaging and contour mapping, and digital image processing applied to sonar data.

He was guest editor of the October 1989 special issue of IEEE JOURNAL OF OCEANIC ENGINEERING. He is a member of the Acoustical Society of America and the American Geophysical Union.